SAE TECHNICAL PAPER SERIES

2008-36-0058

E

DOI: 10.4271/2008-36-0058

Performance Prevision of a Turbocharged Natural Gas Fuelled S.I. Engine

Emiliano Pipitone
Department of Mechanics, University of Palermo, Italy

Francesco Cagnes
Department of Mechanics, University of Palermo, Italy

Alberto Beccari
Department of Mechanics, University of Palermo, Italy

SAE BRASIL
Sociedade de Engenheiros da Mobilidade

FILIADA À
SAE International

Congresso 2008
SAE BRASIL

XVII Congresso e Exposição Internacionais da Tecnologia da Mobilidade
São Paulo, Brasil
07 a 09 de outubro de 2008

2008-36-0058

Performance Prevision of a Turbocharged Natural Gas Fuelled S.I. Engine

Emiliano Pipitone
Francesco Cagnes
Alberto Beccari
Department of Mechanics, University of Palermo

ABSTRACT

Natural gas represents today maybe the most valid alternative to conventional fuels for road vehicles propulsion. The main constituent of natural gas, methane, is characterized by a high autoignition temperature, which makes the fuel highly resistant to knocking: this allows a considerable downsizing of the engine by means of supercharging even under high compression ratio. Starting from these considerations, the authors realized a thermodynamic model of a 4-cilynder s.i. engine for the prevision of in-cylinder pressure, employing a two-zone approach for the combustion and adding sub-models to account for gas properties change and knocking occurrence. An extensive experimental campaign has been carried out on the test bed, equipped with a naturally aspirated bi-fuel s.i. engine (i.e. an engine which can run either with gasoline or with compressed natural gas), so as to set the model constants to the best matching values. Hence the model has been modified adding a turbocharger sub-model, thus allowing a prevision of the power and fuel consumption attainable by the same CNG engine when turbocharged.

INTRODUCTION

One of the most promising alternative to conventional fuel for road vehicles is nowadays represented by natural gas, a mixture whose main constituent is methane, a fuel characterized by a high autoignition temperature; this makes natural gas highly resistant to knocking and would allow a considerable downsizing of s.i. engine by means of supercharging even under high compression ratio. The authors, starting from this considerations, aimed to evaluate the performance achievable by turbocharging a series production engine fuelled with natural gas, without any other modification in the engine structure, i.e. without increasing the number of inlet valves or changing the compression ratio.

To the purpose the authors build-up a thermodynamic model of the engine, simple enough to allow reliable simulations without strong computational effort. The model, realized as a block diagram under Simulink-MatLab, was conceived in two main parts: the engine core, whose task is to simulate the in-cylinder thermodynamic process, and the outer system, whose task is to simulate the phenomena regarding the mass flow in the inlet and discharge systems. The outer system was realized by means of the “lumped component” technique, i.e. the characteristics of every single components were taken into consideration with a stand alone elements; thus a single duct is represented by two distinct block: one to simulate the inertia effect of the fluid flow and the other one to account for its capability to accumulate fluid mass.

Fig. 1 represents the structure of the entire engine model, whose single elements will be described in the following section.

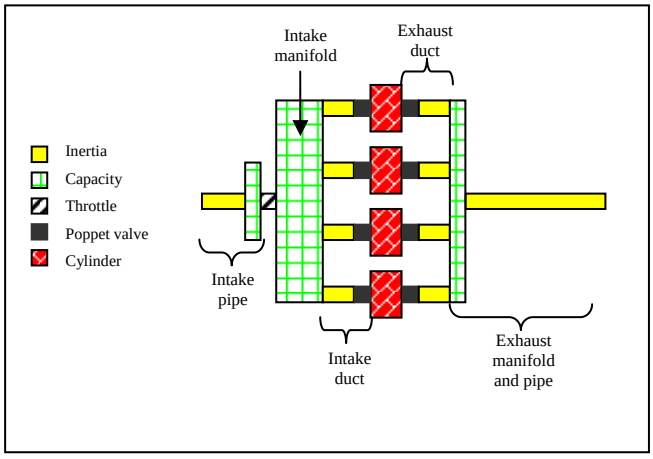

Fig. 1 – engine model diagram

The model has been tuned by means of experimental data acquired on the test bed equipped with a FIAT four cylinder 8V bi-fuel (i.e. capable to run either with gasoline or with natural gas) S.I. engine.

MODEL BLOCKS DESCRIPTION

As shown in Fig. 1, the main blocks of the engine model are the inertia, the capacity, the pressure loss, the cylinder.

The "**inertia**" block simulates the inertia that the fluid mass opposes to every speed change. It is described as a portion of a duct of constant area A and length l (see Fig. 2) inside which the fluid is considered with constant density ρ (hence mass variation is not allowed). The equations used in this element (see Fig. 2) are:

$$(p_1 - p_2)\cdot A = m\frac{dc}{dt} = \rho A l \frac{dc}{dt} \qquad 1)$$

where p_1 and p_2 represent the fluid pressure at inlet and outlet of the inertia duct. The integration of equation (1) gives the inside fluid speed c.

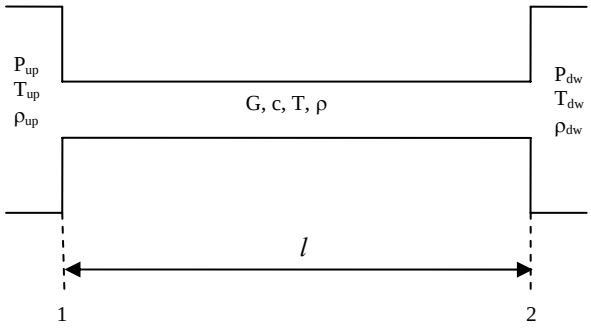

Fig. 2 – Element "inertia"

In the model realized each inertia block is inserted between two capacity blocks. The flow from the upstream capacity is considered hydraulic, i.e. with constant density, while the flow into the downstream capacity has been considered isobaric, i.e. the whole kinetic energy is lost.

For each "inertia" duct the gas flow rate is:

$$G = \rho A c \qquad 2)$$

The "**capacity**" block has the purpose to account for the mass variation which may occurs inside each real duct or manifold. The inside gas has been considered as a perfect gas, hence:

$$p = \rho R' T \qquad 3)$$

being p, ρ and T the gas pressure, density and temperature, while R' represents the gas constant.

The gas density and temperature are obtained integrating respectively the mass conservation equation and the first law of thermodynamics (see Fig. 3):

$$G_{in} - G_{out} = \frac{dm}{dt} = V\frac{d\rho}{dt} \qquad 4)$$

$$\frac{dU}{d\vartheta} = \frac{\delta Q}{d\vartheta} + \frac{G_{in}}{\omega}\left(i_{in} + \frac{c_{in}^{\ 2}}{2}\right) - \frac{G_{out}}{\omega}\left(i_{out} + \frac{c_{out}^{\ 2}}{2}\right) \qquad 5)$$

where ω denotes the engine angular velocity, dU represents the internal energy variation and δQ the heat transferred in the rotation $d\vartheta$. The subscripts *in* and *out* refer to the inlet and outlet quantities.

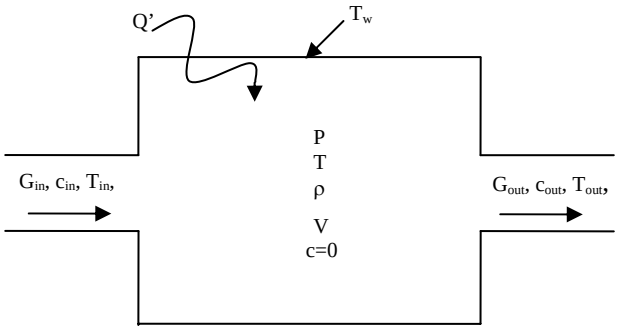

Fig. 3 – Element "capacity"

Once the internal energy variation dU is known, the gas temperature can be evaluated: in fact

$$\frac{dU}{d\vartheta} = m\frac{du}{d\vartheta} + u\frac{dm}{d\vartheta} = mc_v\frac{dT}{d\vartheta} + \frac{u}{\omega}(G_{in} - G_{out}) \qquad 6)$$

hence

$$\frac{dT}{d\vartheta} = \frac{\frac{dU}{d\vartheta} - \frac{u}{\omega}(G_{in} - G_{out})}{mc_v} \qquad 7)$$

the specific heat c_v, the specific internal energy u, and the specific enthalpy i were evaluated, for each chemical species, by means of the polynomial expression reported on the JANAF tables [1].

The same quantities were evaluated for the gas mixture as an average weighted over the mass concentration.

The "**pressure loss**" blocks were used to model the behavior of those elements used to control the mass flow and characterized by non negligible pressure losses, such as the throttle valve or the poppet valves.

As concern the throttle valve, the experimental data available showed that for each throttle position the volumetric flow rate $V°$ correlates to the total pressure drop ΔP across the valve (see Fig. 4) by means of a simple power law:

$$V^{\circ} = a \cdot \Delta P^{b} \qquad 8)$$

where a and b are two constant depending on the throttle

position; equation (8) hence allows the evaluation of the mass flow rate between the intake pipe and the intake manifold.

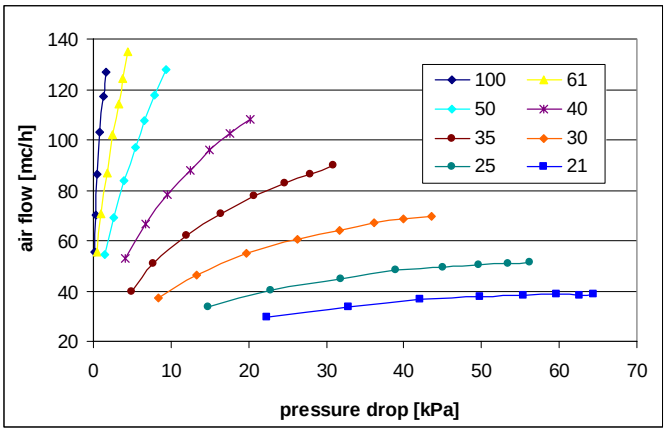

Fig. 4 – Volumetric flow rate as function of the throttle valve pressure drop for different valve rotation percentage

As regards the flow through the poppet valves, the dissipation phenomena have been taken into account through the use of the following discharge coefficient:

$$C_d = \frac{c_{real}}{c_{ideal}} = \frac{c_{curt}}{\sqrt{\frac{2 \cdot \Delta P_{valve}}{\rho_{curt}} - c_{up}^2}} \qquad 9)$$

where c_{up} is the upstream gas speed, while ρ_{curt} and c_{curt} represent the gas density and speed in the valve curtain area $A_{curt} = \pi\, d_v\, h_v$, being d_v and h_v the valve diameter and lift. The gas density in the curtain area has been computed on the base of the upstream density corrected for pressure and temperature changes, while the curtain gas speed has been deduced by the mass flow computed in the connected inertia duct (see eq. 2):

$$G = (\rho \cdot c \cdot A)_{curt} = (\rho \cdot c \cdot A)_{duct} \qquad 10)$$

Eq. (9) then allow to evaluate the pressure drop across each valve once known the gas flow rate:

$$\Delta P_{valve} = \frac{\rho_{curt}}{2}\left[\left(\frac{c_{curt}}{C_d}\right)^2 - c_{up}^2\right] \qquad 11)$$

this pressure loss is taken into account in the evaluation of the gas acceleration inside the inertia duct: as example, equation (1) become:

$$(p_1 - p_2 - \Delta P_{valve}) = m\frac{dc}{dt} = \rho\, l\frac{dc}{dt} \qquad 12)$$

Failing experimental data regarding the discharge coefficients of the engine considered, the authors decided to set these values so as to obtain a good matching between the volumetric efficiency evaluated by the model and the one evaluated at the engine test bed.

CYLINDER SUB-MODEL

The main element of the entire model is represented by the cylinder block which is interested by important processes of mass and energy exchange. The combustion process was simulated by means of a two zone model which will be described forward. As for the "capacity" block, the main equation refer to the mass conservation:

$$m_{cil}(\vartheta) = m_0 + \int_0^{\vartheta}(G_{in} - G_{out})\frac{1}{\omega}d\vartheta \qquad 13)$$

and to the first law of thermodynamics:

$$\frac{dU}{d\vartheta} = \frac{\delta Q_{st}}{d\vartheta} - p\frac{dV}{dt} + \frac{G_{in}}{\omega}\left(i_{in} + \frac{c_{in}^2}{2}\right) - \frac{G_{out}}{\omega}\left(i_{out} + \frac{c_{out}^2}{2}\right) \qquad 14)$$

The heat δQ_{st} received by the gas from in-cylinder wall surface S during the rotation $d\vartheta$ is:

$$\frac{\delta Q_{st}}{d\vartheta} = \frac{h_w\, S\,(T_{wall} - T)}{\omega} \qquad 15)$$

where T_{Wall} is the cylinder wall temperature, while the heat transfer coefficient h_W has been represented by means of the Woschni model [2], hence:

$$h_W = F_w \cdot D^{-0,2} P^{0,8} c_W{}^{0,8} T^{-0,55} \qquad 16)$$

being D the cylinder bore, c_W the gas velocity and F_W a calibration coefficient, determined as the best matching value between simulation and experimental data.

THE COMBUSTION MODEL – The combustion has been simulated by a two zone approach, thus taking into consideration separately both the burnt and the unburnt gas evolution.

The model is an adaptation of those proposed by Blizard e Keck [3] with successive modification [4], [5], [6]: the combustion is characterized by the propagation of a spherical flame front which, starting from the spark electrode, proceeds with a turbulent speed c_f entraining the unburned mixture; the entrained gas then burns with laminar speed c_l in the characteristic time τ_b which depends on a characteristic eddies dimension λ_τ [5]

$$\tau_b = \frac{\lambda_\tau}{c_l} \qquad 17)$$

where the eddies dimension can be evaluated as:

$$\lambda_\tau = Cr \cdot h_i \cdot \left(\frac{\rho_{ivc}}{\rho_u}\right)^{0.5} \qquad 18)$$

here h_i represents the instantaneous height of combustion chamber, ρ_{ivc} the gas density at Intake Valve Closure (IVC), while *Cr* is a calibration constant of the model.

The flame front propagation speed is composed as follows [6]:

$$c_f = c_l + \left(\frac{\rho_u}{\rho_b}\right)^2 \cdot \left(1 - e^{-\frac{R_f}{\lambda_\tau}}\right) u' \qquad 19)$$

being R_f the flame front radius, u' a turbulent parameter, expressed by the calibration coefficient *Ct* as:

$$u' = Ct \cdot n \qquad 20)$$

while c_l represents the laminar flame speed [9]

$$c_l = c_{l_0}\left(\frac{T_u}{T_0}\right)^{\alpha} \cdot \left(\frac{p_0}{p}\right)^{1/\beta}\left(1 - 1.5\phi_r\right) \qquad 21)$$

estimated as a function of the residual gas fraction ϕ_r, of the laminar flame speed c_{lo} of CNG, at standard conditions T_0 and p_0 for different A-F ratio, and of actual gas temperature and pressure by means of the two coefficient α and β depending on pressure and temperature respectively.

$$\alpha = 1.986 + 0.014 \cdot p \qquad 22)$$

$$\beta = 2 + 0.001 \cdot T \qquad 23)$$

If A_f is the flame front surface and ρ_u the unburnt gas density, the mass entrainment rate and the mass burning rate are:

$$\frac{dm_e}{d\vartheta} = \frac{\rho_u A_f c_f}{\omega} \qquad 24)$$

$$\frac{dm_b}{d\vartheta} = \frac{1}{\omega}\left(\frac{m_e - m_b}{\tau_b}\right) \qquad 25)$$

to which corresponds the heat released rate

$$\frac{dQ_{comb}}{d\vartheta} = \frac{dm_b}{d\vartheta}\left(1 - \phi_r\right)\frac{H_i}{\alpha + 1} \qquad 26)$$

where *Hi* is the fuel lower heat value.

The flame front surface A_f is analytically obtained evaluating the intersection of a sphere of radius R_f with the cylinder walls. Both the piston and the head surface were considered flat (as in the real engine on the test bench).

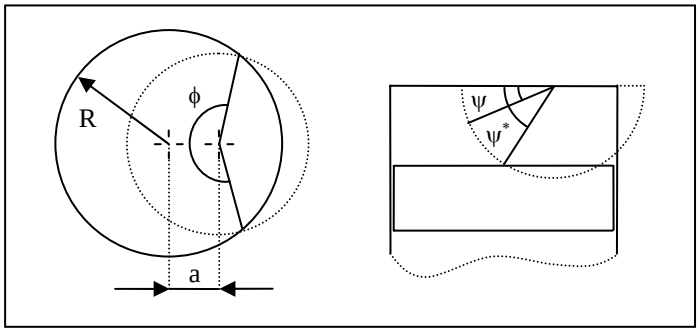

Fig. 5 – integration angles for A_f evaluation

$$A_f = 2R_f^{\,2}\int_o^{\psi^*} \varphi \cdot \cos\psi \cdot d\psi \qquad 27)$$

where φ and ϑ are integration angles as shown in Fig. 5, and then:

$$\varphi = \arccos\left[\frac{a^2 + \left(R_f \cos\psi\right)^2 - R^2}{2aR_f \cos\psi}\right] \qquad 28)$$

where *a* is the spark electrode eccentricity, while the radius R_f has been calculated taking into account the entraining speed, the burning gas expansion and the volume variation caused by the piston motion; hence the entrained volume rate of change is:

$$\begin{aligned}\frac{dV_e}{d\vartheta} &= A_f \frac{dR_f}{d\vartheta} + A_{cs}\frac{dh_i}{d\vartheta} = \\ &= A_f \frac{dR_f}{d\vartheta} + 4\frac{A_{cs}}{\pi D}\frac{dV}{d\vartheta}\end{aligned} \qquad 29)$$

where A_{cs} is the piston contact area and $\frac{dV_e}{d\vartheta}$ is obtained considering that the total in-cylinder volume is known:

$$V_e = V_b + \frac{m_e - m_b}{\rho_u} \qquad 30)$$

The equation set is completed by the first law of thermodynamics, the mass and volume conservation, and the perfect gas law applied to both burnt and unburnt gas:

$$m_b + m_u = m_{cil}\,; \qquad V_b + V_u = V_{cil} \qquad 31)$$

$$\rho_b R'_b T_b = p_b = p_u = \rho_u R'_u T_u = p \qquad 32)$$

$$\frac{dU_b}{d\vartheta} = \frac{\delta Q_{stb}}{d\vartheta} + \frac{\delta Q_{comb}}{d\vartheta} - p\frac{dV_b}{d\vartheta} + i_u \frac{dm_b}{d\vartheta} \qquad 33)$$

$$\frac{dU_u}{d\vartheta} = \frac{\delta Q_{stu}}{d\vartheta} - p\frac{dV_u}{d\vartheta} - i_u\frac{dm_b}{d\vartheta} \quad 34)$$

$$\frac{dU_b}{d\vartheta} = u_b\frac{dm_b}{d\vartheta} + m_b c_{vb}\frac{dT_b}{d\vartheta} \quad 35)$$

$$\frac{dU_u}{d\vartheta} = u_u\frac{dm_u}{d\vartheta} + m_u c_{vu}\frac{dT_u}{d\vartheta} \quad 36)$$

and finally:

$$\frac{dT_b}{d\vartheta} = \frac{\left[\frac{\delta Q_{stb}}{d\vartheta} + \frac{\delta Q_{comb}}{d\vartheta} - p\frac{dV_b}{d\vartheta} - (i_u - u_b)\frac{dm_b}{d\vartheta}\right]}{m_b c_{vb}} \quad 37)$$

$$\frac{dT_u}{d\vartheta} = \frac{1}{m_u c_{vu}}\left(\frac{\delta Q_{stu}}{d\vartheta} - p\frac{dV_u}{d\vartheta} - R'T_u\frac{dm_b}{d\vartheta}\right) \quad 38)$$

The heat transferred to burned (δQ_{stb}) and unburnt gas (δQ_{stu}) were evaluated by means of the Woschni model [2], Eq. (15) and (16), computing the respective heat exchange surfaces, function of the flame radius R_f.

In order to detect possible abnormal and dangerous combustion, a model for knocking prevision was employed [11]: by means of an Arrhenius type correlation, ignition retard τ is evaluated depending on the thermodynamics state of unburned gas during both compression and expansion stroke:

$$\tau_{[s]} = 0.911\cdot 10^{-3}\left(\frac{O.N.}{100}\right)^{3.402} p_{[MPa]}^{-1.7}\, e^{\frac{3800}{T_{[K]}}} \quad 39)$$

where O.N. represents the octane number of the fuel.
According to the authors of the model [11], the following integral reaches the value of 1 when the auto ignition condition is achieved, i.e.:

$$\int_{t_{IVC}}^{t_{knock}} \frac{1}{\tau}dt = \int_{\vartheta_{IVC}}^{\vartheta_{knock}} \frac{1}{\tau}\frac{d\vartheta}{\omega} = 1 \quad 40)$$

The authors of the present paper adopted this model since it confirmed two experimental condition, resumed in Table 1:

Fuel used	RPM	MAP	λ	$T_{manifold}$	Knock
Gasoline	1500	70 kPa	1.0	35°C	Yes
Natural gas	1000	100 kPa	1.0	100°C	No

Table 1 – Operative condition used to tune the knocking prevision model constant

As shown, knocking was caused easily during gasoline operation, while with natural gas, due to its high knock resistance (O.N. ≈125) and the relative low compression ratio of the engine on the test bench (9.8), no knocking phenomena were observed even under the worst condition. The authors of the paper then modified the model constant (which was set to 0.911) in order to consider the second condition of Table 1 as an incipient knock condition: this make the knocking prevision model conservative.

CALIBRATION OF COMBUSTION MODEL – The coefficient *Ct* and *Cr* were tuned by means of mass fraction burned curves evaluated applying the Rassweiler & Withrow method [12] on experimental pressure cycles, acquired at full load in order to minimize the influence of residual gas. It was found *Ct=0.75* and *Cr=1.75* as the best matching values.

Once fixed the combustion model constant, the authors tuned the heat transfer model constant F_W by means of other pressure cycles acquired for different operative conditions of speed and load; simulated and experimental pressure curves were compared in terms of indicated mean effective pressure (IMEP) considering only the compression and expansion strokes, so as to ignore any difference in the pumping cycles.

Fig. 6, Fig. 7 and Fig. 8 show some results of the model compared to the experimental data: as can be observed, a good matching was obtained in terms of MFB, pressure cycle and IMEP estimation (the maximum difference is 1.5% at 2000 rpm).

TURBOCHARGING SUB-MODEL

Once the model has been set-up for the naturally aspirated engine, the authors focused on the introduction of the turbocharger model.

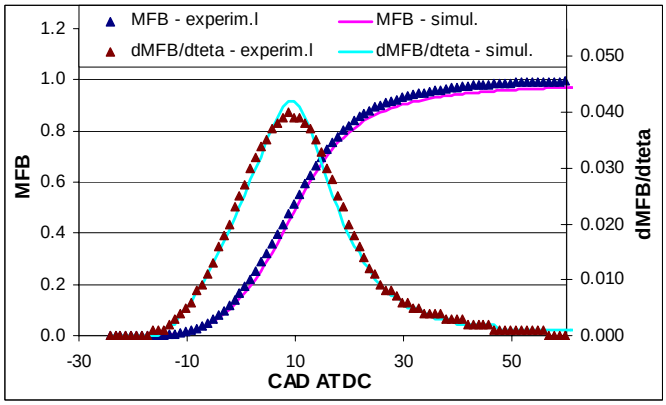

Fig. 6 – Simulated and experimental MFB at 3000 RPM, λ=1.00, WOT, SA=26°

To this purpose, some modifications to the original model were necessary: as can be observed in Fig. 9, the turbocompressor, which was supposed to take air at ambient condition (1 bar, 300 K), is followed by a duct, modeled as a pure "capacity" for its high volume; this, in turn, is followed by an intercooler, introduced in order to lower the gas temperature, which is connected to the throttle body; the intercooler has been simulated by means of both "inertia" and "capacity" block; on the exhaust side, the only modification regarded the introduction of the turbine between the exhaust manifold (pure "capacity") and the final exhaust pipe (endowed of both "capacity" and "inertia")

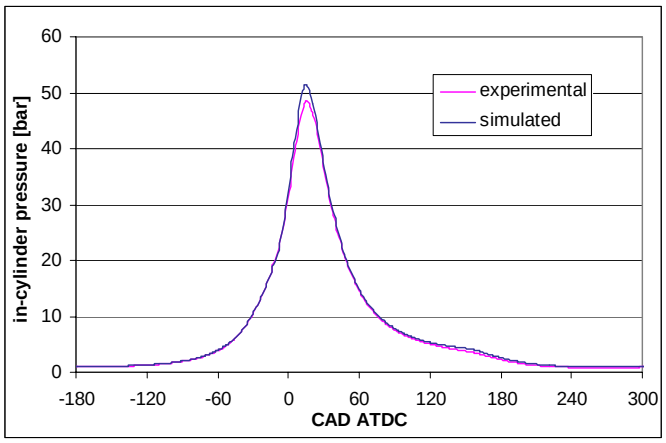

Fig. 7 – Cylinder pressure at 3500 RPM, λ=1.00, WOT SA=26°

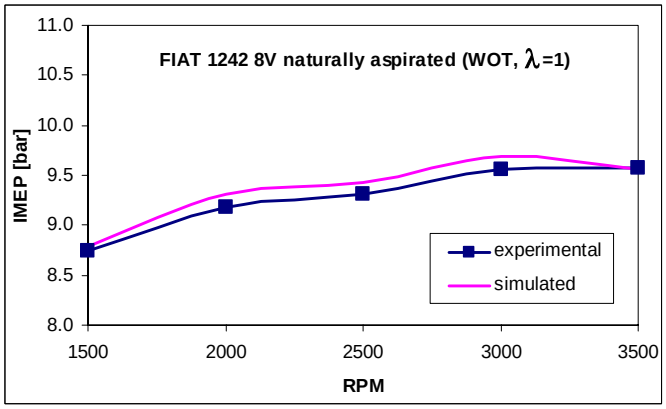

Fig. 8 – *Imep* comparison at WOT, λ=1.00

The turbocharger here considered is the IHI RHF3, which has been modeled using the turbocompressor operating map, gently provided by IHI, and the turbine operating map, derived from well detailed data available in literature [13].

The compressor map was implemented in SimuLink, in order to evaluate its mass flow rate and efficiency for given compression ratio (known from the boundary condition) and rotor revolution speed, derived from the rotor power balance equation:

$$P_T - P_C = I_R \cdot \omega_R \cdot \alpha_R = I_R \cdot \omega_R \cdot \frac{d\omega_R}{dt} \qquad 41)$$

where P_T and P_C represent the power generated by the turbine and required by the compressor respectively, I_R is the inertia moment of the turbocharger rotor, while ω_R and α_R are the rotor angular velocity and acceleration.

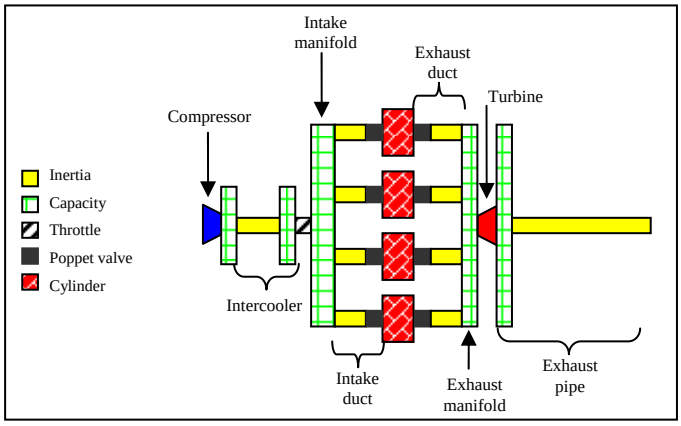

Fig. 9 – turbocharged engine model diagram

The same approach was used to model the turbine, whose mass flow rate and efficiency were deduced from the maps shown in Fig. 10 and Fig. 11, for given expansion ratio (known from the boundary condition) and rotor speed.

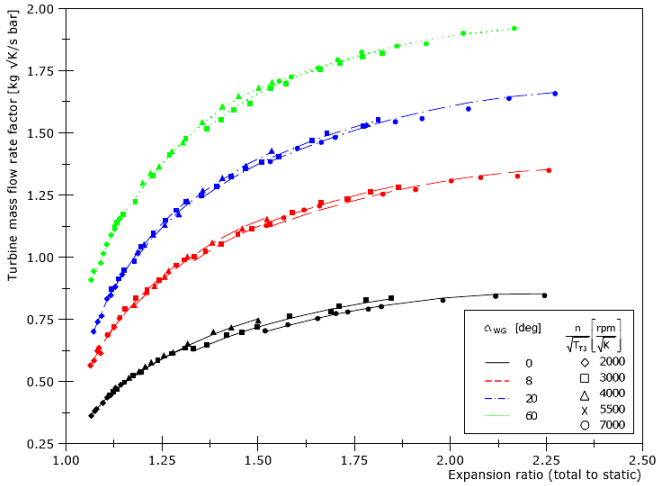

Fig. 10 – turbine characteristic map [13]

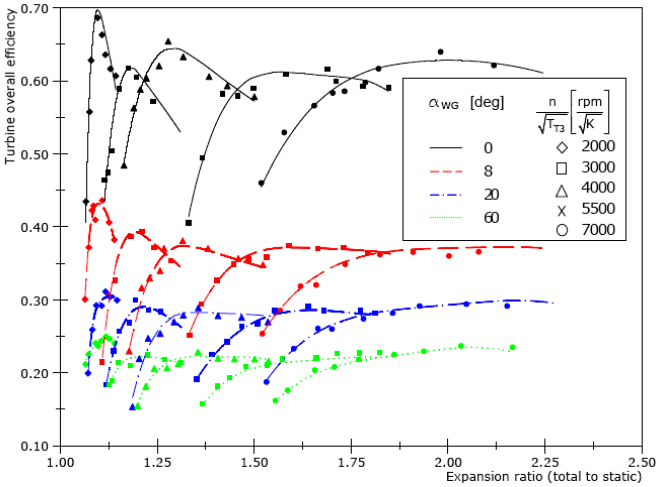

Fig. 11 – turbine efficiency map [13]

Moreover, the data reported on these turbine maps were acquired on a flow test bench for different waste-gate valve openings, hence allow a precise estimation of turbine mass flow and efficiency for each condition. It is worth to mention that the values reported on these maps refer to the expansion of the whole mass flowing through the turbine system, i.e. the turbine rotor and waste-gate.

Analyzing the map in Fig. 10 it was observed a proportionality between the mass flow rate and the waste-gate opening degree for each expansion ratio; this allowed to trace the diagram in Fig. 12 which reports the mass flow increment, with respect to the condition of closed waste-gate, as function of the opening degree, apart from the expansion ratio.

The authors of the present paper then used the overall fitting exponential correlation to evaluate the turbine system mass flow for each waste-gate opening.

A similar approach was followed also for the efficiency map of Fig. 11; another proportionality factor was determined (see Fig. 13), which allowed to express the turbine system overall efficiency with respect to the closed waste-gate condition, as function of the waste-gate openings apart from the expansion ratio. Hence the turbine performance implementation required the mass flow and the efficiency data for closed waste-gate valve, together with the mass flow factor and the efficiency factor.

As already discussed, an intercooler was inserted between the turbocompressor outlet and the manifold to lower air temperature, so as to maximize engine performance without causing knocking to occur.

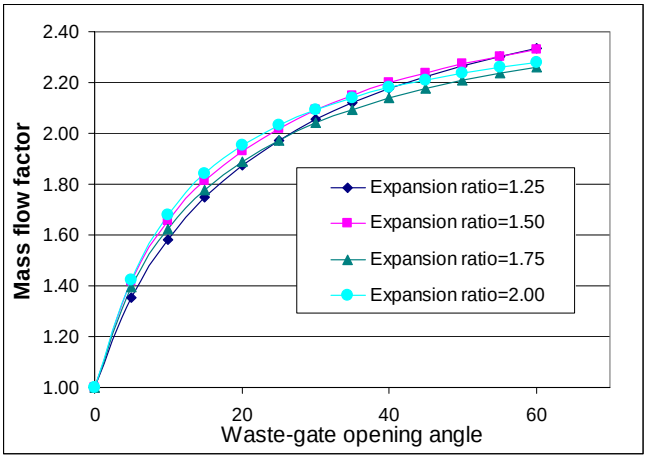

Fig. 12 – amplification coefficient of gas flow rate

The intercooler taken into consideration is a MODINE 188AE.TCA.D, characterized by a heat exchange surface S_{int} of about 1.39 m^2; it was modelled as an "inertia" block followed by a "capacity": the first to take account of the inertia effects inside the small inner duct, where the gas reach the speed of 20 m/s, while the second to take account of its great volume (2.3 litre).

The power exchanged by the intercooler has been evaluated as:

$$\frac{\delta Q_{\text{int}}}{d\vartheta} = \frac{h_{\text{int}}\, S_{\text{int}}\, \Delta T_{ml}}{\omega} \qquad 42)$$

where ΔT_{ml} expresses the mean logarithmic temperature difference, function of the maximum and minimum temperature difference between the cold and hot gas:

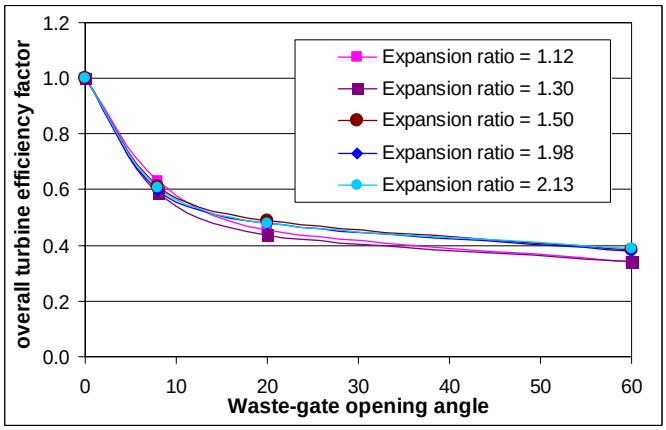

Fig. 13 – Turbine efficiency factor vs waste-gate opening angle

$$\Delta T_{ml} = \frac{\Delta T_{\max} - \Delta T_{\min}}{\ln\left(\frac{\Delta T_{\max}}{\Delta T_{\min}}\right)} \qquad 43)$$

The heat exchange coefficient h_{int} was determined by means of experimental data and correlated to the inner gas speed by means of 2nd order polynomial. Before its final implementation, the intercooler performance were successfully verified against the experimental data.

To complete the model, a friction mean effective pressure (*fmep*) model was introduced, so as to evaluate the effective engine output. The authors choose the classical approach of the Chen-Flynn model:

$$fmep = A + B \cdot p_{\max} + C \cdot n + D \cdot n^2 \qquad 44)$$

whose constant were tuned on the base of experimental data acquired for the naturally aspirated engine on the test bed with varying speed, manifold pressure and spark timing.

RESULTS

As a result of the two models realized, the authors evaluated the performances of both the naturally aspirated and the turbocharged engine, whose waste-gate valve was set to start opening for a manifold pressure of 1.9 bar (this maintained the turbocharger speed below its maximum allowable), and to be fully opened at 2.5 bar. Fig. 14 shows the two indicated mean effective pressure curves as function of engine speed at full load: the IMEP increase exceed the 80% from 2500 to 5500 rpm. The same diagram also reports the manifold pressure resulted from the turbocharged simulation: as shown, the turbocompressor reaches the 1.9 bar supercharging pressure beginning at 2500 rpm. According to

the "knocking prevision" model, none of the operative condition simulated was characterized by knocking, even if the unburned gas reached the peak pressure of 116 bar (at 4000 rpm) and the temperature of 1000 K.

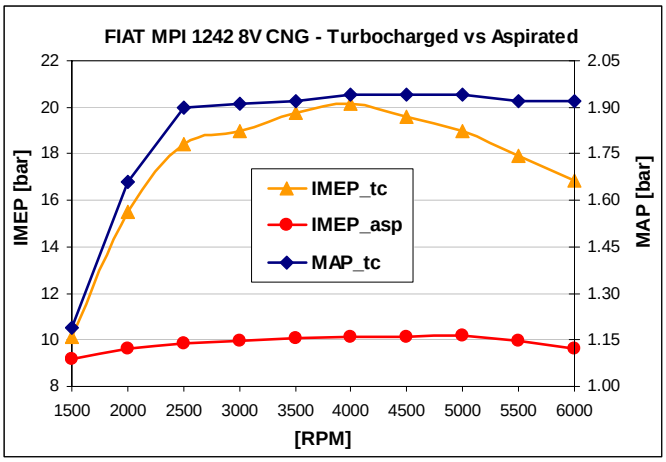

Fig. 14 – IMEP - Comparison between turbocharged and naturally aspirated

Fig. 15 shows the engine torque and power evaluated at WOT for both the naturally aspirated and the turbocharged engine. As shown, the simulation predicts the maximum engine torque to increase from 88 Nm at 3000 rpm to 186 Nm at 4000 rpm (to which corresponds a BMEP of 19 bar), while the maximum engine power should pass from 48 kW at 6000 rpm to 93 kW at 6000 rpm.

Fig. 16 reports the evaluated brake specific fuel consumption (BSFC) as function of engine speed at full load; as can be observed the specific consumption of the turbocharged unit is always lower than that of the aspirated one, whose minimum is 245 g/kWh; the turbocharged engine results to maintain a consumption lower than 220 g/kWh from 2500 to 4500 rpm.

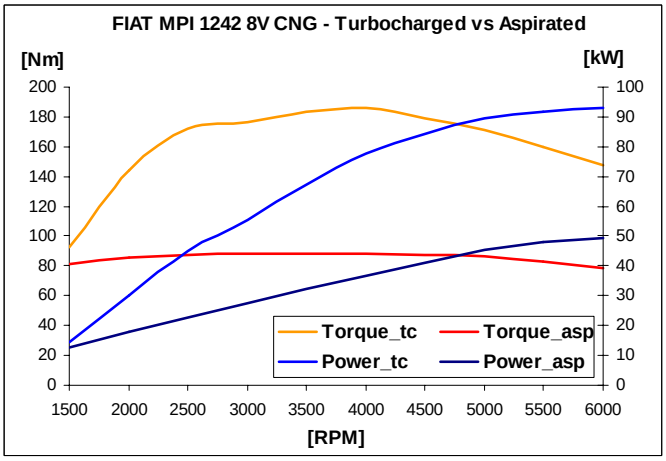

Fig. 15 – Engine torque and power - comparison between turbocharged and naturally aspirated

CONCLUSION

The authors of the paper realized a thermodynamic model of a four cylinder spark ignition engine fuelled with natural gas on the base of a experimental data collected on the engine test bed equipped with a FIAT bi-fuel engine. The combustion has been simulated using a two zone model, while the intake and exhaust systems were modeled with the "lumped parameter" approach. The model was then calibrated and verified by means of different experimental data. Hence it was modified in order to evaluate the performance attainable by means of turbocharging and intercooling the inlet air, considering a waste-gate actuation manifold pressure of 1.9 bar.

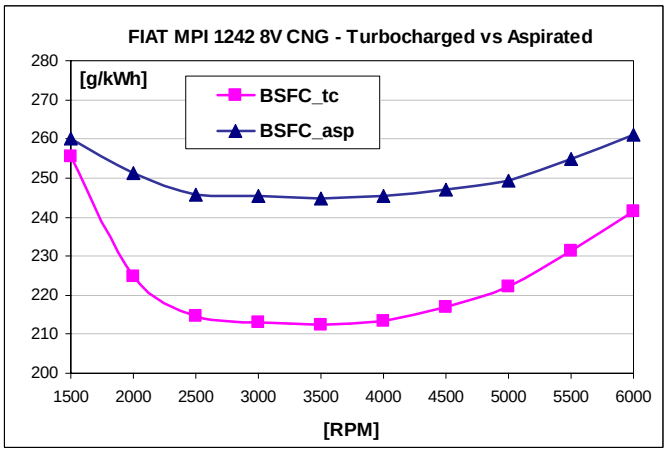

Fig. 16 – Brake specific fuel consumption - comparison between turbocharged and naturally aspirated

A "knocking prevision" model was also introduced to identify possible abnormal and dangerous combustion. The results obtained by the naturally aspirated engine model showed a good matching with the experimental data, in terms of indicated mean effective pressure. The naturally aspirated and the turbocharged engine models were than compared in terms of resulting IMEP, torque, power and fuel consumption. The comparison showed increment on engine torque and power of 110% and 88% respectively, while the minimum fuel consumption was found to decrease by about a 13%.

AKNOWLEDGEMENT

The authors express their gratitude to Prof. Emilio Catania from Politecnico di Torino and to Ing. Andrea Gerini from *Fiat Powertrain Technologies* who made this work possible, to Ing. Perego at *IHI* for the information and the data provided, and to Mr. Beniamino Drago for its invaluable technical support.

REFERENCES

[1] NIST-JANAF, "Thermochemical Tables, Fourth Edition," Journal of Physical and Chemical Reference Data, M.W. Chase JR, 1998.

[2] G. Woschni, "A Universally Applicable Equation for the Instantaneous Heat Transfer Coefficient in the Internal Combustion Engine," SAE Trans., Vol. 76, pp. 3065-3083,

1967.

[3] N.C. Blizard, J. C. Keck, “Experimental and Theoretical Investigation of Turbulent Burning Model for Internal Combustion Engines,” SAE paper 740191, SAE Trans., Vol. 83, 1974.

[4] J.C. Keck, J.B. Heywood, G. Noske, “Early Flame Development and Burning Rates in Spark Ignition Engines,” SAE paper 870164, SAE Trans., Vol. 96, 1987.

[5] R.J. Tabaczynski, C.R. Ferguson, K. Radhakrishnan, “A Turbulent Entrainment Model for Spark-Ignition Engine Combustion,” SAE paper 770647, SAE Trans., Vol. 86, 1977.

[6] D.D. Brehod, C.E. Newman, “Monte Carlo Simulation of Cycle by Cycle Variability,” SAE paper 922165, 1992.

[7] M. Metghalchi, J.C. Keck, “Laminar Burning Velocity of Propane-Air Mixtures at High Temperature and Pressure,” Combustion and Flame, Vol. 38, pp.143-154, 1980.

[8] M. Metghalchi, J.C. Keck, “Burning Velocities of Mixtures of Air with Methanol, Isocatne and Indolene at High Pressure and Temperature,” Combustion and Flame, Vol. 48, pp. 191-210, 1982.

[9] L. Bromberg, "In-Cylinder Laminar Flame Propagation Speed: Effect of Hydrogen And Hydrogen Rich Gas Addition", PSFC/JA-05-21, August 26 2005, MIT Plasma Science and Fusion Center

[10] D. Rhodes, J.C. Keck, Laminar Burning Speed Measurements of Indolene-Air-Diluent Mixtures at High Pressures and Temperatures,” Proc. SAE, pp. 23-35, 1985.

[11] W.S. Wayne, N.N. Clark, C.M. Atkinson, “Numerical Prediction of Knock in a Bi-Fuel Engine,” SAE paper 982533, 1998.

[12] G.M. Rassweiler, L. Withrow, “Motion Pictures of Engine Flames Correlated with Pressure Cards,” SAE Journal, Vol. 42(May), pp. 185–204, 1938.

[13] M. Capobianco, S. Marelli, “Waste-Gate Turbocharging Control in Automotive SI Engines: Effect on Steady and Unsteady Turbine Performance,” SAE paper 2007-01-3543

ABBREVIATIONS AND SYMBOLS

ATDC	After Top Dead Centre
asp	naturally aspirated
BTDC	Before Top Dead Centre
CAD	Crank angle degee
CNG	compressed natural gas
MAP	Manifold Absolute Pressure
O.N.	Octane number
S.I.	spark ignition
tc	turbocharged

m	mass
p	pressure
T	temperature
ρ	density
R'	gas constant
c_p	constant pressure specific heat
c_v	constant volume specific heat
d	infinitesimal difference
d_v	valve diameter
Δ	finite difference
ΔP	pressure drop
δ	infinitesimal quantity
k	specific heat ratio c_p/ c_v
h_v	valve lift
l	length
A	cross section area
S	surface
V	volume
$V°$	volumetric gas flow rate
I	moment of inertia
c	speed
G	mass flow rate
t	time
ϑ	crankshaft angle
ω	angular velocity
Q'	thermal power
Q	heat
L	indicated work
U	internal energy
u	specific internal energy
i	specific enthalpy
h	heat transfer coefficient
K	adimensional pressure loss coefficient
TPS	throttle position sensor
A_0	throttle plate section area
$C_{1,2...}$	numeric constant or coefficient
D	bore
h_i	combustion chamber instantaneous height
R_f	flame front radius
A_f	flame front spherical surface
F_w	Woschni model calibration coefficient
C_t , C_r	combustion model calibration coefficient
IVC	intake valve closure

SUBSCRIPTS

0	initial or total upstream state
$1, 2,...$	cross section 1,2,… state
up	upstream
dw	downstream
in	inlet
out	outlet
is	isentropic
cil	cylinder
st	heat exchange
w	Woschni
r	reference state
mot	motored
s	piston
u	unburnt
b	burnt

e	entrained
comb	combustion
l	laminar
f	flame front
t	turbine
c	compressor
R	turbocharger rotor
int	intercooler
ml	logarithmic mean